Acta Cryst. (1977). A33, 723–729

A Study of the Electron-Density Distribution in Sodium Azide, NaN_3

BY E. D. STEVENS* AND H. HOPE

Department of Chemistry, University of California, Davis, California, 95616, USA

(*Received* 9 *August* 1976; *accepted* 10 *March* 1977)

The crystal structure of sodium azide, NaN_3, has been reinvestigated by X-ray diffraction methods. The electron density of the azide ion as determined using a high-order X-ray refinement is compared with the theoretical density determined in an *ab initio* molecular-orbital calculation. The wavefunction of the azide ion has been used to calculate improved atomic scattering factors which result in a significant improvement in the refinement. Molecular scattering factors calculated from the wavefunction have been used in rigid-body refinements including librational thermal motion. The molecular refinement results in a significantly better fit than do the atomic refinements. When standard ellipsoidal temperature factors are used false detail is indicated in deformation-density maps. This problem is eliminated when a third-cumulant expansion is used.

Introduction

When accurate X-ray data are combined with parameters from the refinement of neutron data or high-order X-ray data, the distribution of electron density in the structure can be determined experimentally. One of the goals of such studies is the comparison of theoretical calculations of the molecular electron density with experiment. Reliable theoretical densities require calculations with extensive basis sets (Cade, 1972). Such calculations are presently practical only for small molecules.

Parameters refined from high-order X-ray data show little bias from valence density features since the scattering at high angles is due primarily to the core electrons. In various stages of development these ideas have been advocated or applied by, for example, Stewart (1968), Furberg & Jensen (1970), Little, Pautler & Coppens (1971), Stevens & Hope (1975). In order to obtain sufficient X-ray data for a high-order refinement the thermal motion of the atoms must be small. This can be achieved by lowering the temperature or by choosing a structure with low thermal motion at room temperature.

The structure of sodium azide was chosen for reinvestigation since it was expected to have low thermal motion. In addition, the azide ion is small enough that rigorous quantum mechanical calculations are feasible. Since the start of this work, the results of a neutron diffraction study have become available (Choi & Prince, 1976).

Experimental

Sodium azide (Schering-Kahlbaum AG) was recrystallized from a 95% ethanol solution by slow evaporation of solvent, giving plates with a thickness of about 0·25 mm. Preliminary Weissenberg photographs indicated twinning, with the minor component ranging from about 1 to 10%, depending on the specimen. With hexagonal indexing of the space group $R\bar{3}m$, the condition for reflection is $-h+k+l=3n$ (n integer). Reflections from the minor component of the twin obeyed the apparent condition $h-k+l=3n$, which corresponds to a change in the sign of the c axis. Twinning is probably caused by stacking faults along the **c** direction.

Since we found no untwinned crystals, X-ray intensities were measured from both components of a twinned crystal. A crystal for data collection was cut in a 0·3 × 0·4 mm rectangular section from a plate 0·2 mm thick and mounted in an arbitrary orientation. The setting angles of 16 Mo $K\alpha_1$ reflections were carefully measured and used in a least-squares determination of the unit-cell dimensions and crystal orientation. The cell dimensions were found to be $a=3{\cdot}646$ (1) and $c=15{\cdot}223$ (3) Å.

For reflections with indices such that $h-k=3n$, symmetry-related reflections from both parts of the twin overlap. It was necessary to collect intensities from both and combine the intensities of symmetry-related reflections which did not overlap. The size of the minor component was about 5% of the crystal. Raw counts were merged before further data reduction. A preliminary set of low-order data was first collected and refined. In order to obtain sufficient high-order data without spending time measuring large numbers of weak reflections, the preliminary structure was used to predict which reflections would have measurable intensities.

The intensities of 210 unique reflections which were predicted to be observable were measured in the range $0{\cdot}0<\sin\theta/\lambda<1{\cdot}3$ Å^{-1} on a Picker card-controlled diffractometer using a θ:2θ scan and monochromatic Mo $K\alpha$ radiation. Each reflection was scanned from $[2\theta(\alpha_1)-1{\cdot}00°]$ to $[2\theta(\alpha_2)+1{\cdot}00°]$ with a 2θ scan speed of 0·5° min^{-1}. Background counts were collected for 100 s at each end of the scan. Coincidence losses were

* Present address: Department of Chemistry, State University of New York, Buffalo, NY 14214, USA.

diminished by automatically adding attenuator foils and remeasuring the reflections whenever the count rate exceeded 10^4 counts s^{-1}. The intensities of two check reflections were measured every 50 reflections and showed no significant changes during data collection.

For each number of counts N, a standard deviation $\sigma(N)$ was assigned from the expression $\sigma(N)=[N+(0{\cdot}004N)^2]^{1/2}$, where the term $0{\cdot}004N$ reproduces the observed variances of the intensities of the check reflections.

The values of $\sigma(N)$ were used to calculate estimated standard deviations for the net intensities and observed structure factors. Reflections with $I>\sigma(I)$ were considered observed and used in further calculations and refinements. Lorentz and polarization corrections were applied to the data.

Scattering factors

Atomic scattering factors calculated from relativistic Hartree–Fock (HF) wavefunctions were taken from Doyle & Turner (1968). Scattering factors calculated from Slater-type orbitals (STO) with exponents optimized to the calculated electron distribution in small molecules (Stewart, 1970) were used in some refinements.

An *ab initio* molecular orbital calculation was performed on the azide ion with a minimal basis set of Gaussian orbitals, introduced by Whitten (1966). The basis set consisted of three *s*-type orbitals and three *p* orbitals for each of the N atoms. The separation between N nuclei was chosen to be 2·2087 a.u. (1·169 Å).

The converged wavefunctions gave a total energy of −162·94960 a.u., which is slightly lower than the energies reported by Clementi & McLean (1963) and by Bonaccorsi, Petrongolo, Scrocco & Tomasi (1968) for calculations using STO basis sets. Subsequently, Archibald & Sabin (1971) have reported extensive calculations on the N_3^- ion using a larger Gaussian basis set. They found a minimum in the total energy at an internuclear separation of 2·220 a.u. (1·175 Å) and report a lowest variational energy of −163·198 a.u.

The wavefunctions calculated for the azide ion have been used to calculate molecular X-ray scattering factors. The scattering from a molecule is given by

$$f(\mathbf{S})_{\rm mol}=\int \varrho(\mathbf{r})\exp(i\mathbf{S}\cdot\mathbf{r})d\mathbf{r} \qquad (1)$$

where ϱ is the ground-state electron density, $\mathbf{S}$ is the scattering vector, and $\mathbf{r}$ is the position vector.

Atomic scattering factors for N give a poor approximation to the scattering from the azide ion at low angles. There is an additional electron in the azide ion which is distributed primarily at the ends of the molecule. In order to get a better model for the azide ion and keep the simple spherical atom formalism, a least-squares calculation was performed to give the best spherical-atom scattering factor (BSAF) fit to the molecular scattering. The quantity minimized was

$$\sum_{hkl} w^2\Big[\sum_i f_i \exp(i\mathbf{S}\cdot\mathbf{R}_i)-f(\mathbf{S})_{\rm mol}\Big]^2 \qquad (2)$$

where $\mathbf{R}_i$ is the distance to the ith atom.

The atomic scattering factors are expressed as a sum of Gaussian terms

$$f_i=\sum_{j=1}^{4} A_{ij}\exp[-B_{ij}(\sin\theta/\lambda)^2]+C_i \qquad (3)$$

and the A_{ij}, B_{ij}, and C_i are variables in the refinement.

The values of $f(\mathbf{S})_{\rm mol}$ were included for 525 values of h, k, l to a $\sin\theta/\lambda$ of 1·40 $Å^{-1}$. A weighting factor

$$w=\exp(-\sin\theta) \qquad (4)$$

was used for each 'observation'. Since the parameters are highly correlated, it was necessary to alternately refine the A_{ij} and C_i with B_{ij} fixed, and then refine B_{ij} with A_{ij} and C_i fixed. The refinement was started with A_{ij}, B_{ij}, and C_i values for a relativistic Hartree–Fock N atom.

The agreement between the molecular scattering factor and the atomic scattering factors is expressed as

$$R=\sum_{hkl}\big||f(\mathbf{S})_{\rm mol}|-|\sum_i f_i\exp(i\mathbf{S}\cdot\mathbf{R}_i)|\big|/\sum_{hkl}|f(\mathbf{S})_{\rm mol}| \qquad (5)$$

and

$$R_w=\sum_{hkl} w^2(|f(\mathbf{S})_{\rm mol}|-|\sum_i f_i\exp(i\mathbf{S}\cdot\mathbf{R}_i)|)^2/\sum_{hkl} w^2 f(\mathbf{S})^2_{\rm mol}. \qquad (6)$$

After 36 cycles, the refinement had converged at $R=4{\cdot}62\%$ and $R_w=3{\cdot}28\%$. The largest deviation from $f(\mathbf{S})_{\rm mol}$ was 0·62 e. The large values of R and R_w are an indication of the inability of the spherical-atom model to fit the scattering from the azide ion. A similar least-squares fit of one spherical atom to the scattering from the wavefunctions of a N atom gave $R=0{\cdot}03\%$ and $R_w=0{\cdot}02\%$.

The parameters for the best spherical atom fit (BSAF) scattering factors determined by this procedure are listed in Table 1. A comparison of the BSAF scattering factors with the HF scattering factor for N is given in Fig. 1.

Table 1. *Coefficients for Gaussian terms giving scattering factors for end,* N(1), *and central,* N(2), *nitrogen atoms*

	N(1)	N(2)
A_1	2·969198	17·617764
B_1	0·065580	0·068413
A_2	3·059980	3·602899
B_2	10·091955	8·409583
A_3	2·948577	1·180461
B_3	27·519820	50·492425
A_4	0·806566	−2·439186
B_4	0·687508	0·476359
C	−1·914169	−13·659762

The detailed form of (1) suggests an approach to refining X-ray data using molecular scattering factors. The basis functions φ_j of the molecular orbitals are expressed in terms of a sum of Gaussian lobe functions

$$\varphi_j=\sum_m A_{jm}\exp(-B_{jm}\mathbf{r}_m^2) \quad (7)$$

where A_{jm} and B_{jm} are constants and the subscript on $\mathbf{r}_m$ indicates that the center of the mth lobe does not necessarily coincide with the center of the atom (Whitten, 1966). The molecular orbitals are given by

$$\psi_i=\sum_j C_{ij}\varphi_j\,, \quad (8)$$

where the C_{ij}'s have been determined in the theoretical calculations, and the total density ϱ by

$$\varrho(\mathbf{r})=\sum_i n_i(\psi_i)^2 \quad (9)$$

where n_i is the occupation number of the ith molecular orbital.

Substituting (7), (8), and (9) into (1), and integrating gives

$$f(\mathbf{S})_{\mathrm{mol}}=\sum_i n_i\sum\sum C_{ij}C_{ik}\sum_m\sum_n A_{jm}A_{kn}I_{jkmn} \quad (10)$$

where

$$I_{jkmn}=\exp\left[-\frac{B_{jm}B_{kn}}{(B_{jm}+B_{kn})}\mathbf{R}_{mn}^2+i\mathbf{S}\,.\,\mathbf{R}_p\right]\times\left\{\left[\frac{\pi}{(B_{jm}+B_{kn})}\right]^{3/2}\exp-\left[\frac{\mathbf{S}^2}{4(B_{jm}+B_{kn})}\right]\right\}. \quad (11)$$

In the simplification of (1), the point P has been introduced which lies on the line between centers of Gaussian lobes m and n such that $B_{jm}|\mathbf{R}_{mp}|=B_{kn}|\mathbf{R}_{np}|$. Expression (10) for $f(\mathbf{S})_{\mathrm{mol}}$ is equivalent to the corresponding expressions derived by McWeeny (1953) and by Groenewegen & Feil (1969). The evaluation of the molecular scattering factor is much more difficult when Slater orbitals are used.

The general expression for the scattering contribution of an atom j located at a point $\mathbf{r}_j$ in the unit cell is

$$F_j=f_j\exp(i\mathbf{S}\,.\,\mathbf{r}_j) \quad (12)$$

where f_j is the atomic scattering factor. Each term in (10) acts as if it were a scattering source at the point $\mathbf{r}_j=\mathbf{R}_p$ with scattering power $f_j=C''_{mn}\exp(-\mathbf{S}^2D_p)$ where

$$C''_{mn}=\sum_{jk} C'_{jk}A_{jm}A_{kn}\exp\left[-\frac{B_{jm}B_{kn}}{(B_{jm}+B_{kn})}\mathbf{R}_{mn}^2\right]\times\left[\frac{\pi}{(B_{jm}+B_{kn})}\right]^{3/2}, \quad (13)$$

$$C'_{jk}=\sum_i n_iC_{ij}C_{ik} \quad (14)$$

and

$$D_p=\left[\frac{1}{4(B_{jm}+B_{kn})}\right]. \quad (15)$$

These expressions can also be used to refine the rigid-body librational motion of a molecule as well as the translational motion with the form of the anisotropic librational temperature factor derived by Pawley & Willis (1970).

In least-squares refinement with molecular scattering factors, each term in (11) has been treated as if it were a scattering source and all librational terms in the first, second, and third cumulant expansion (Pawley & Willis, 1970) included.

In a calculation of $f(\mathbf{S})_{\mathrm{mol}}$, initially the values of C''_{mn}, D_p, and the x, y, and z components of $\mathbf{R}_p$ are computed and stored. If C''_{mn} is zero, then it is not necessary to store the other values for a particular m, n combination. Values of $f(\mathbf{S})$ can then be quickly calculated for any value of $\mathbf{S}$ by summing over m and n. For sodium azide there are only 3070 unique m, n combination with non-zero contributions to $f(\mathbf{S})_{\mathrm{mol}}$ in the basis set used.

Refinement

Initial parameters in the least-squares refinement were taken from Pringle & Noakes (1968). Each reflection was weighted by $w=1/\sigma^2(F)$ where $\sigma(F)$ is the estimated standard deviation of F_o.

The data were divided into two groups: a low-order group with 69 unique observed reflections in the range $0{\cdot}0<\sin\theta/\lambda<0{\cdot}65$ Å^{-1} and a high-order group with 139 unique observed reflections in the range $0{\cdot}65<\sin\theta/\lambda<1{\cdot}25$ Å^{-1}.

The results of conventional refinement with HF, STO, and BSAF scattering factors are given in Table 2. Neutron diffraction results (Choi & Prince, 1976) are included for comparison. Because all the atoms lie on a threefold axis the anisotropic temperature factors are required to have only two unique components. Since the Na atom and the central N of the azide molecule also lie on inversion centers (site symmetry $\bar{3}m$), their coordinates are fixed. The Na atom is at (0, 0, 0) and the center N, N(2), at (0, 0, $\frac{1}{2}$). The only

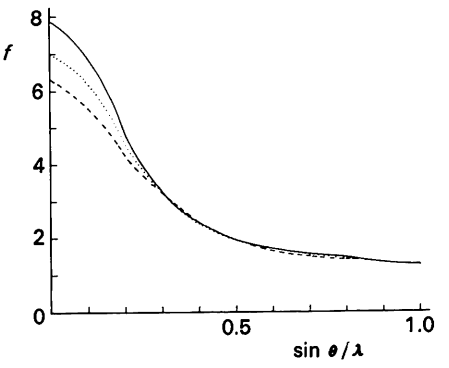

Fig. 1. Comparison of spherical best-fit form factors. End N (——), central N (----) and neutral RHF N (···).

Table 2. *Results of refinements with ellipsoidal temperature factors*

Scattering factor	HF	HF	STO	STO	BSAF	BSAF	Neutron
sin θ/λ range (Å^{-1})	0·0–0·65	0·65–1·25	0·0–0·65	0·65–1·25	0·0–0·65	0·65–1·25	
Number of parameters	8	8	8	8	8	8	8
Number of reflections	69	139	69	139	69	139	145
R(%)	2·04	3·95	2·24	3·93	1·70	4·00	2·9
R_w(%)	3·61	2·57	3·04	2·54	2·35	2·56	2·7
Goodness of fit	12·5	2·15	10·0	2·12	8·55	2·13	
Scale	0·02822 (26)	0·02944 (11)	0·02841 (22)	0·02920 (11)	0·02801 (18)	0·02890 (11)	
Na							
B_{11}	2·699 (52)	2·538 (27)	2·645 (44)	2·554 (26)	2·723 (36)	2·572 (27)	2·41 (9)
B_{33}	2·043 (73)	1·897 (23)	1·963 (60)	1·912 (23)	2·044 (49)	1·927 (23)	1·69 (9)
N(1)							
z	0·57688 (14)	0·57681 (5)	0·57715 (12)	0·57682 (5)	0·57640 (10)	0·57681 (5)	0·57654 (6)
B_{11}	3·536 (82)	3·543 (29)	3·592 (70)	3·510 (29)	3·549 (57)	3·589 (29)	3.41 (4)
B_{33}	1·750 (84)	1·586 (19)	1·742 (71)	1·556 (18)	1·975 (60)	1·635 (19)	1·57 (4)
N(2)							
B_{11}	1·795 (76)	1·975 (25)	1·843 (64)	1·923 (25)	1·876 (52)	1·947 (25)	1·83 (4)
B_{33}	2·206 (124)	1·654 (21)	2·065 (103)	1·626 (21)	1·955 (82)	1·646 (21)	1·52 (4)

Table 3. *Results of third-cumulant refinements*

Scattering factor	HF	HF	STO	STO	BSAF	BSAF
sin θ/λ range (Å^{-1})	0·0–0·65	0·65–1·25	0·0–0·65	0·65–1·25	0·0–0·65	0·65–1·25
Number of parameters	11	11	11	11	11	11
Number of reflections	69	139	69	139	69	139
R(%)	2·05	2·61	1·67	2·66	1·53	2·87
R_w(%)	3·21	1·70	2·10	1·69	1·90	1·77
Goodness of fit	11·4	1·43	7·48	1·42	6·76	1·48
Scale	0·2819 (5)	0·02981 (4)	0·02838 (5)	0·02942 (7)	0·02799 (5)	0·02910 (7)
Na						
B_{11}	2·698 (48)	2·551 (4)	2·645 (31)	2·565 (18)	2·724 (29)	2·584 (19)
B_{33}	2·076 (67)	1·868 (11)	2·005 (43)	1·890 (15)	2·025 (39)	1·906 (16)
N(1)						
z	0·57734 (20)	0·57667 (11)	0·57777 (13)	0·57676 (13)	0·57598 (11)	0·57681 (14)
B_{11}	3·569 (76)	3·477 (17)	3·630 (51)	3·479 (19)	3·528 (45)	3·559 (20)
B_{33}	1·634 (83)	1·587 (9)	1·611 (55)	1·558 (12)	2·022 (49)	1·637 (13)
C_{111}	0·0169 (189)	0·0253 (30)	0·0245 (127)	0·0247 (40)	0·0191 (112)	0·0244 (41)
C_{333}	0·1305 (312)	0·0099 (47)	0·1594 (205)	0·0115 (50)	−0·0849 (209)	0·0133 (54)
C_{113}	−0·0140 (156)	−0·0225 (21)	−0·0035 (103)	−0·0194 (25)	−0·0172 (92)	−0·0180 (26)
N(2)						
B_{11}	1·608 (105)	1·932 (11)	1·658 (70)	1·895 (25)	1·905 (65)	1·932 (27)
B_{33}	2·546 (152)	1·604 (12)	2·425 (97)	1·586 (14)	1·825 (77)	1·608 (15)

positional parameter is that of the end N, N(1), along the threefold axis at (0, 0, z).

The results of third cumulant refinements are given in Table 3. All third cumulant parameters are required to be zero for site symmetry $\bar{3}m$. The end N with site symmetry $3m$ has three unique elements in the third cumulant tensor. All of the third cumulant refinements lead to significant improvements to the fit at the 0·005 significance level as judged by Hamilton's (1965) R factor ratio test.

Table 4. *Results of molecular, rigid-body refinements*

sin θ/λ range (Å^{-1})	0·0–0·65	0·65–1·25
Number of parameters	5	5
Number of reflections	69	139
R (%)	2·28	5·24
R_w (%)	2·90	4·08
Goodness of fit	9·84	3·44
Scale	0·02790 (20)	0·03039 (56)
Na^+		
B_{11}	2·770 (42)	2·456 (44)
B_{33}	2·029 (57)	1·839 (39)
N_3^-		
B_{11}	1·832 (56)	1·989 (43)
B_{33}	2·024 (61)	1·560 (29)
L_{11}	0·0148 (11)	0·0139 (7)

The results of a least-squares refinement using molecular scattering factors are given in Table 4. The parameters derived from a rigid-body fit to the atomic thermal parameters obtained from conventional refinements with HF scattering factors are given in Table 5. The rigid body fit of the azide ion was calculated using the procedure derived by Schomaker & Trueblood (1968). The libration component L_{11} determined by neutron diffraction is 0·0150 (4).

Table 5. *Parameters from rigid body fit to atomic thermal parameters*

N_3^-	Low order	High order
B_{11}	1·800 (150)	1·958 (24)
B_{33}	1·903 (87)	1·611 (16)
L_{11}	0·0161 (19)	0·0147 (1)

Table 6 gives a listing of h, k, l, $100kF_o$, $100F_c$, and $10w$. The values of F_c were calculated from the parameters determined in the conventional high-order refinement (Table 2) with HF scattering factors. Reflections below a sin θ/λ of 0·65 Å^{-1} are marked with the letter L. Reflections below 0·65 Å^{-1} which were considered unobserved are marked with the letter U.

Table 6. *Observed and calculated structure factors*

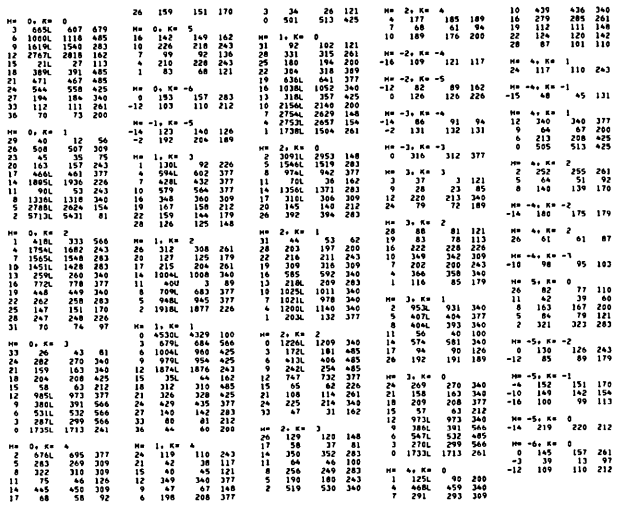

Discussion

The results of a conventional refinement (Table 2) show that it is difficult to predict the effect the valence-electron distribution will have on the low-order refinement. The position of the terminal N might be expected to change to compensate for the increased distribution of electrons in the bonding region of the azide ion. However, no significant difference is found in the N–N bond lengths between high and low-order refinements.

The thermal parameter of the central N along the bond (B_{33}) is significantly larger than the corresponding thermal parameters of the end N atoms. Considering the intra- and intermolecular force constants it is unreasonable to expect the central atom to be vibrating more than the terminal atoms in the azide ion. The large thermal parameter is apparently the result of an attempt by the least-squares procedure to compensate for the electron distribution between the atoms. Although the same thermal parameters are more nearly equal in the high-order refinement, the difference is still about six standard deviations.

Although the value of R is lower in the low-order refinement, the much smaller goodness of fit value for the high-angle data is an indication of fewer model errors in the high-order refinement. As with other compounds (Stevens & Coppens, 1975), the low-order scale factor is smaller than the high-order scale factor. Various scale factors are compared in Table 7.

Table 7. *Scale factors obtained from different procedures*

X-ray refinements	Scale factor
HF scattering factors	
Low-order data	0·0282 (3)
High-order data	0·0294 (1)
STO scattering factors	
Low-order data	0·0284 (2)
High-order data	0·0292 (1)
BSAF scattering factors	
Low-order data	0·0280 (2)
High-order data	0·0289 (1)
Molecular scattering factors	
Low-order data	0·0279 (2)
High-order data	0·0304 (6)
Refinement of scale only, full data	
Neutron parameters, HF scattering factors	0·0300 (1)
High-order X-ray parameters, HF scattering factors	0·0291 (1)
Average experimentally measured scale (Stevens & Coppens, 1975)	0·0291 (3)

As expected, refinement with STO atomic scattering factors improves the agreement between the high and low-order scale factors. Both refinements give lower goodness of fit values. However, the agreement between N B_{33} temperature factors is not improved. The low-order refinement is significantly improved when BSAF scattering factors are used. The R value decreases to 1·7% and the goodness of fit to 8·55. Both the low and high-order N B_{33} values agree within one estimated standard deviation. The agreement between high and low-order scale factors is almost the same as when STO scattering factors are used.

Refinement with third-cumulant parameters (Table 3) results in a significant improvement in the agreement between the data and the model. The R and R_w values and goodness of fit are lower. The high-order N B_{33} thermal parameters agree within less than 2σ. Third-cumulant refinements with STO and BSAF scattering factors give the best fit with $R=1{\cdot}53\%$ and $R_w=1{\cdot}90\%$ and a goodness of fit of 6·76. The third-cumulant refinement with STO scattering factors gives the best fit to the high-order data with $R=2{\cdot}66\%$ and $R_w=1{\cdot}69\%$ and a goodness of fit of 1·42. The agreement between high and low-order scale factors is worse in all the third cumulant refinements.

A fourth cumulant refinement of the high-order data with HF scattering factors gave $R=2{\cdot}59\%$ and $R_w=1{\cdot}67\%$ but because of the number of additional parameters introduced, this does not correspond to a significant improvement.

Refinements using scattering factors calculated from the molecular wavefunctions rather than atomic scattering factors have been carried out on the structure of ammonium fluoride by Groenewegen & Feil (1969) and on the structure of diborane by Jones & Lipscomb (1970). The present study is the first molecular refinement to include the librational thermal motion of the molecule.

The low-order refinement using molecular scattering factors for the azide ion gives better agreement with fewer parameters than the conventional refinements with HF and STO atomic scattering factors. The improvement of the BSAF refinement over the molecular refinement is only slightly more than expected from the increased number of parameters.

The high-order molecular refinement is significantly poorer than all of the conventional atomic refinements. The results would certainly be improved if the N–N bond length were optimized. The site symmetry of the molecule requires that all translational third-cumulant terms be zero, so a molecular refinement with third-cumulant thermal parameters is not possible.

The librational parameter L_{11} determined in the molecular refinement is in good agreement with the value determined from a rigid body fit to the individual high-order atomic thermal parameters (Table 5) and with the value refined from neutron diffraction data.

Comparison of X-ray parameters (Table 2) with neutron parameters reveals significant differences even when high-order refinements and improved scattering factors are used. The neutron thermal parameters are systematically lower than the X-ray values. The parameters from high-order refinements are generally closer to the neutron values than the low-order parameters.

A computer-drawn plot of the theoretical difference density in the azide ion is given in Fig. 2. This map was calculated by subtracting the sum of the three N atomic densities from the molecular density at each point. The relatively large lone pairs and lack of density in the bonding region can be attributed to the lack of flexibility in the basis set (Cade, 1972) and has also been noted in a theoretical study of cyanuric acid (Jones, Pautler & Coppens, 1972). Before the experimental density maps can be compared with a thermally smeared version of the theoretical density, such as Fig. 2, much better theoretical calculations are required. Comparison of experimental results with an extended-basis-set calculation will be described elsewhere (Stevens, Rys & Coppens, 1977*a*, *b*).

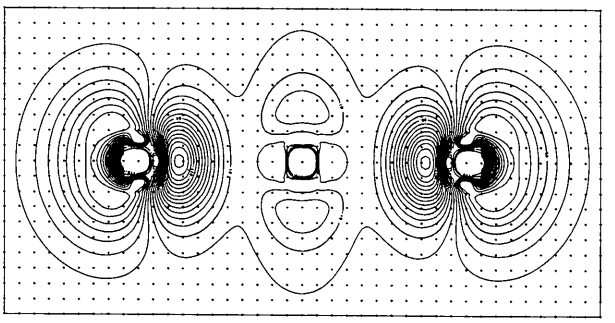

Fig. 2. Theoretical deformation map.

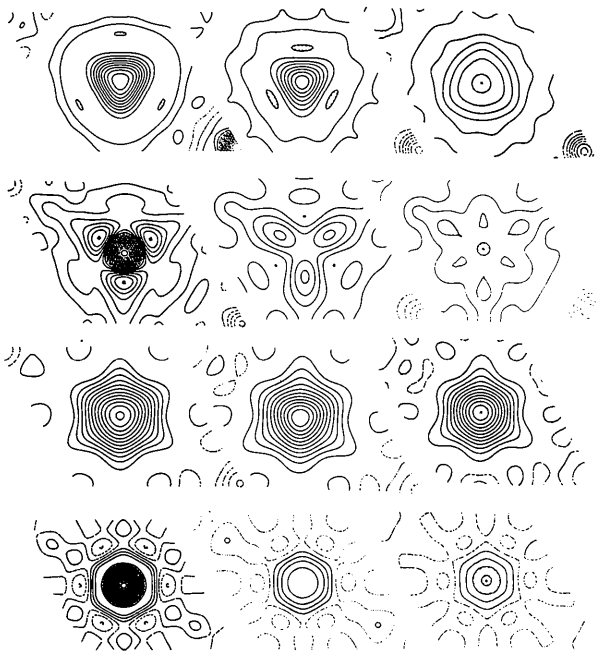

(*a*) (*b*) (*c*)

Fig. 3. Valence electron deformation maps for N_3^-, sections normal to axis of ion. (*a*) $X-N$, (*b*) $X-X_{\text{high order}}$, second cumulant, (*c*) $X-X_{\text{high order}}$, third cumulant. Top row: sections through lone pair, 0·28 Å from end N. Second row: sections through end N. Third row: sections through center of N–N bond. Bottom row: sections through central N.

The reliability of experimental deformation-density maps depends critically on the adequacy of the model on which the calculation of $\Delta F=F_o-F_c$ is based. Of foremost significance is the accuracy of the description of the thermal motion. The present study gives a clear illustration of this point. We have prepared plots of ϱ_{X-N} using neutron parameters, (Choi & Prince, 1976) with second-cumulant temperature factors, the full X-ray data set, HF scattering factors and the experimentally measured scale factor; the plots are shown in Figs. 3(*a*) and 4(*a*). Plots of $\varrho_{X-X_{\text{high order}}}$ were also prepared; one set using the second-cumulant temperature factors [Figs. 3(*b*) and 4(*b*)], and another set using the third-cumulant temperature factors from the same data [Figs. 3(*c*) and 4(*c*)]. In these cases the least-squares scale factors were used.

The $X-N$ and $X-X_{\text{high order}}$ maps based on the second cumulant temperature factor differ mostly in regions near atomic centers, where the value of the scale factor is most likely to give rise to differences in the maps.

The most dramatic changes appear when the third-cumulant parameters are used for F_c, most clearly visible in the vicinity of the end N atom. The second cumulant data would seem to indicate a marked triangular shape to the valence-electron distribution about the end N, including lone pair, with electron density extending into the regions between the Na^+ ions. However, with the third-cumulant calculations this structure disappears. A vaguely triangular shape of the lone pair is observed, but now with electron density extending toward the Na^+ ions.

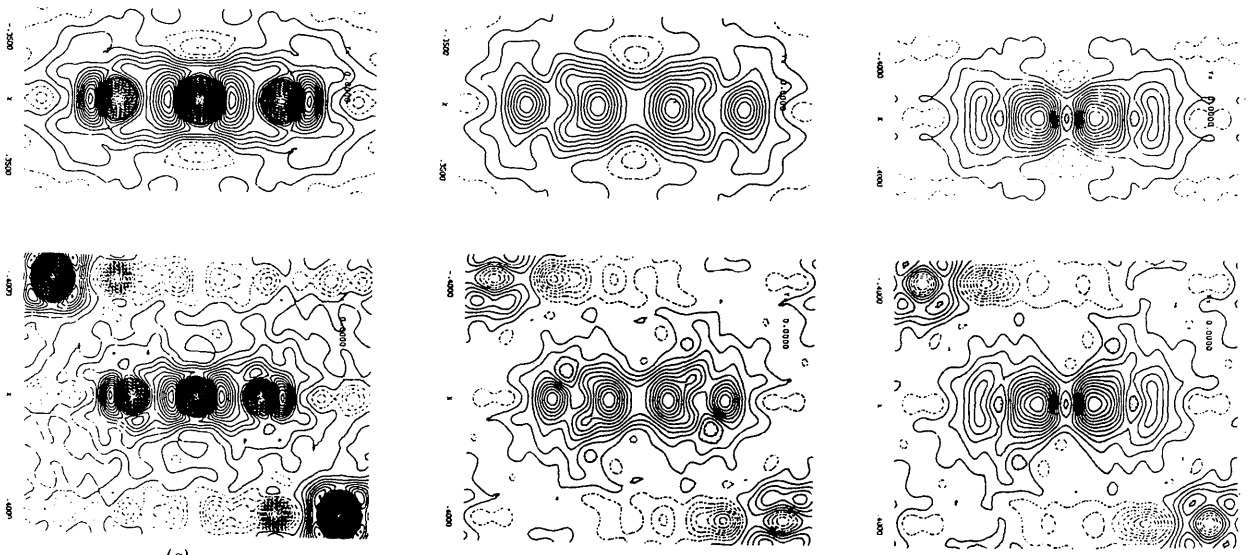

(a) (b) (c)

Fig. 4. Valence electron deformation maps for N_3^-, sections along axis of ion. (a) $X-N$, (b) $X-X_{\text{high order}}$, second cumulant, (c) $X-X_{\text{high order}}$, third cumulant. Top row, plane normal to mirror plane. Bottom row, mirror plane.

These effects seem to be connected with the fact that the azide ion moves in a field of trigonal symmetry. The motion of the end N atom cannot be adequately described by the standard ellipsoidal temperature factor, and when that description is used in the preparation of deformation maps false structure is indicated.

It is clear from this that conclusions regarding valence-electron deformations are not reliable unless the thermal motion description mimics the symmetry of the field in which the atoms or groups in question move.

One of the authors (EDS) gratefully acknowledges receipt of a National Science Foundation Graduate Traineeship. Support of this work by an NSF Grant is also gratefully acknowledged. We thank Drs C. S. Choi and E. Prince for making their neutron results available before publication and Dr W. H. Fink for assistance with the theoretical calculations.

References

ARCHIBALD, T. W. & SABIN, J. R. (1971). *J. Chem. Phys.* **55**, 1821–1829.

BONACCORSI, R., PETRONGOLO, C., SCROCCO, E. & TOMASI, J. (1968). *J. Chem. Phys.* **48**, 1500–1508.

CADE, P. E. (1972). *Trans. Amer. Cryst. Assoc.* **8**, 1–36.

CHOI, C. S. & PRINCE, E. (1976). *J. Chem. Phys.* **64**, 4510–4516.

CLEMENTI, E. & MCLEAN, A. D. (1963). *J. Chem. Phys.* **39**, 323–325.

DOYLE, P. A. & TURNER, P. S. (1968). *Acta Cryst.* A**24**, 390–397.

FURBERG, S. & JENSEN, L. H. (1970). *Acta Cryst.* B**26**, 1260–1268.

GROENEWEGEN, P. P. M. & FEIL, D. (1969). *Acta Cryst.* A**25**, 444–450.

HAMILTON, W. C. (1965). *Acta Cryst.* **18**, 502–510.

JONES, D. S. & LIPSOMB, W. N. (1970). *Acta Cryst.* A**26**, 196–207.

JONES, D. S., PAUTLER, D. & COPPENS, P. (1972). *Acta Cryst.* A**28**, 635–645.

LITTLE, R. G., PAUTLER, D. & COPPENS, P. (1971). *Acta Cryst.* B**27**, 1493–1499.

MCWEENY, R. (1953). *Acta Cryst.* **6**, 631–637.

PAWLEY, G. S. & WILLIS, B. T. M. (1970). *Acta Cryst.* A**26**, 260–262.

PRINGLE, G. E. & NOAKES, D. E. (1968). *Acta Cryst.* B**24**, 262–269.

SCHOMAKER, V. & TRUEBLOOD, K. N. (1968). *Acta Cryst.* B**24**, 63–76.

STEVENS, E. D. & COPPENS, P. (1975). *Acta Cryst.* A**31**, 612–619.

STEVENS, E. D. & HOPE, H. (1975). *Acta Cryst.* A**31**, 494–498.

STEVENS, E. D., RYS, J. & COPPENS, P. (1977*a*). *J. Amer. Chem. Soc.* **99**, 265–267.

STEVENS, E. D., RYS, J. & COPPENS, P. (1977*b*). In preparation.

STEWART, R. F. (1968). *J. Chem. Phys.* **48**, 4482–4889.

STEWART, R. F. (1970). *J. Chem. Phys.* **53**, 205–213.

WHITTEN, J. L. (1966). *J. Chem. Phys.* **44**, 359–364.